# Feasibility Study on the Use of the Coplanar Capacitive Sensing Technique for Underwater Non-Destructive Evaluation

**Martin Mwelango**
China University of Petroleum (East China)
**Xiaokang Yin**
xiaokang.yin@upc.edu.cn
China University of Petroleum (East China)
**Mingrui Zhao**
China University of Petroleum (East China)
**Zhaorui Zhang**
China University of Petroleum (East China)
**Zongkai Han**
China University of Petroleum (East China)
**Ruixiang Fan**
China University of Petroleum (East China)
**Pengcheng Ma**
China University of Petroleum (East China)
**Xin'an Yuan**
China University of Petroleum (East China)
**Wei Li**
China University of Petroleum (East China)

**Research Article**

**Keywords:** Underwater NDE, Coplanar capacitive sensor, Sensitivity distribution field, Negative sensitivity phenomenon, Capacitive imaging

**Posted Date:** March 29th, 2024

**DOI:** https://doi.org/10.21203/rs.3.rs-4137421/v1

**Additional Declarations:** No competing interests reported.

# Feasibility Study on the Use of the Coplanar Capacitive Sensing Technique for Underwater Non-Destructive Evaluation

M. Mwelango[1], X. Yin[2], M. Zhao[3], Z. Zhang[4], Z. Han[5], R. Fan[6], P. Ma[7], X. Yuan[8] and W. Li[9]

[1]National Engineering Research Center of Marine Geophysical Prospecting and Exploration and Development Equipment, China University of Petroleum (East China), Qingdao, 266580, China, mmwelango@yahoo.com, 0000-0002-1426-3501.

[2]National Engineering Research Center of Marine Geophysical Prospecting and Exploration and Development Equipment, China University of Petroleum (East China), Qingdao, 266580, China, xiaokang.yin@upc.edu.cn, 0000-0003-3247-8730.

[3]National Engineering Research Center of Marine Geophysical Prospecting and Exploration and Development Equipment, China University of Petroleum (East China), Qingdao, 266580, China, mingrui.zhao@foxmail.com, 0009-0004-8062-8849.

[4]National Engineering Research Center of Marine Geophysical Prospecting and Exploration and Development Equipment, China University of Petroleum (East China), Qingdao, 266580, China, z21040038@s.upc.edu.cn.

[5]National Engineering Research Center of Marine Geophysical Prospecting and Exploration and Development Equipment, China University of Petroleum (East China), Qingdao, 266580, China, hanzongkai2021@163.com.

[6]National Engineering Research Center of Marine Geophysical Prospecting and Exploration and Development Equipment, China University of Petroleum (East China), Qingdao, 266580, China, ruixiang.fan@foxmail.com.

[7]National Engineering Research Center of Marine Geophysical Prospecting and Exploration and Development Equipment, China University of Petroleum (East China), Qingdao, 266580, China, mpc12152@163.com.

[8]National Engineering Research Center of Marine Geophysical Prospecting and Exploration and Development Equipment, China University of Petroleum (East China), Qingdao, 266580, China, xinancom@163.com, 0000-0003-4849-441X.

[9]National Engineering Research Center of Marine Geophysical Prospecting and Exploration and Development Equipment, China University of Petroleum (East China), Qingdao, 266580, China, liwei@upc.edu.cn, 0000-0002-4121-0456.

*Corresponding author:* xiaokang.yin@upc.edu.cn

# Feasibility Study on the Use of the Coplanar Capacitive Sensing Technique for Underwater Non-Destructive Evaluation


## Abstract

Recent advancements in Non-Destructive Evaluation (NDE) techniques have demonstrated potential in assessing underwater structural integrity. However, evolving maritime structures demand more efficient, user-friendly, and technologically advanced underwater NDE methods. Building on successful applications in air as a medium, this paper explores the feasibility of utilizing coplanar capacitive sensors to gauge structural integrity in underwater environments, drawing on assertions made by pioneering scholars. The study employs simulations, complemented by experimental validation, to assess its viability. With artificial surface defects in both non-conducting and conducting specimens, this study conducts a comprehensive comparison of the performance between the bare-electrode and insulated-electrode Coplanar Capacitive Sensor (CCS). The outcomes affirm the viability of utilizing the technique for underwater NDE. Notably, the study reveals that electrical conductivity is a significantly influential factor, and there are discernible differences in response between the two sensor configurations. The nature of the response in non-conducting materials is intricately tied to the dominant sensitivity value region. However, detecting defects in conducting materials poses a challenge in some instances. Overall, results show that defect detection, characterisation and imaging under water are feasible, thereby emphasizing the techniques potential for underwater NDE. This study broadens underwater NDE knowledge and offers a viable alternative for inspecting structures and equipment in underwater environments.



**Keywords** Underwater NDE, Coplanar capacitive sensor, Sensitivity distribution field, Negative sensitivity phenomenon, Capacitive imaging


## 1. Introduction

In recent years, various NDE techniques have demonstrated their efficacy in gauging the structural integrity of underwater structures. However, with the rapid development of maritime structures, there is an ever-rising demand for underwater NDE techniques with increased efficiency, ease of application, and enhanced technological performance. CCSs have proven invaluable in NDE applications in air. However, their feasibility for underwater inspections remain relatively unexplored. While earlier studies [1,2] suggested the capability of using CCSs underwater, limited published research within the aspect of gauging structural integrity is available. The capacitive sensors have, however, been applied in the field of fluid flow to visualize and monitor fluid flow rate[3], visualize fluid phase changes[4], measure concentration of two-phase flow[5], measure void fraction[6], detect wax deposition[7] and estimate the gas volumetric flow rate[8]. Although these fluid flow applications are categorized under NDE, they do not directly assess structural integrity.

Thus, this paper seeks to address this gap by investigating the feasibility of employing CCSs for underwater NDE, specific to structural integrity through simulations and experiments. Two kinds of CCSs are investigated; the bare-electrode CCS and the insulated-electrode CCS. This feasibility study focuses on detecting artificial defects in less complex conducting and non-conducting materials, specifically perspex and aluminium, immersed in deionized water, followed by tap water and then seawater. This progressive approach

facilitates a comprehensive examination of the impact of varying electrical conductivity levels, providing valuable insights into the adaptability and performance of the capacitive technique under different water environments.

The rest of this paper is organized as follows: Section 2 introduces the applicable principles; Section 3 presents finite element simulation results; Section 4 details experimental outcomes; Section 5 offers a discussion; And section 6 concludes the paper.

## 2. Principles for Underwater NDE using CCS

CCSs are designed with a thin insulation layer covering the electrodes[9]. When the CCS is immersed in a conducting medium, the insulation layer hinders the completion of the electrical circuit, unlike when the electrodes are bare.

The traditional Maxwell's equations[10] are sufficient to model the behavior of both the kinds of CCSs when in air. This is because, for the insulated-electrode CCS, there are two dielectric layers; the insulation layer and the air layer. Similarly, when the insulated-electrode CCS is immersed in water, the traditional Maxwell's equations remain sufficient.

However, when dealing with a bare-electrode CCS immersed in water, the traditional Maxwell's equations are not directly applicable, as they do not account for electrical conductivity. Nevertheless, Bioelectromagnetism offers valuable insights into modelling the behavior of the bare-electrode CCS underwater. Malmivuo and Plonsey[11] identify five distinct phenomena in Bioelectromagnetism that can be leveraged, along with suitable assumptions, to establish a foundation for the modification of the traditional Maxwell's equations. The phenomena include: (1) The behavior of the sources; (2) The electric currents and potentials in the volume conductor; (3) The magnetic field at and beyond the body; (4) How the medium reacts to electric and magnetic field stimulation; (5) The inherent electric and magnetic properties of the sources[11]. With plausible assumptions, the modified Maxwell's equations established by Malmivuo and Plonsey for Bioelectromagnetism are applicable to the case where the bare-electrodes of the CCS are immersed in water. A summary of the derivation as in [11] is given below (Detailed explanations in [11]).

For the first assumption, in line with the first phenomenon, the driving and sensing electrodes are assumed to be the sources of charge from which the electric field arises. The second assumption, in line with the second phenomenon, is that water is assumed to be the volume conductor. Given the dimensions of the CCS and excitation parameters, the effect of magnetic field is negligible; thus, the third phenomenon is not considered. The fourth phenomenon is also not considered, as water is not the object of study. The fifth phenomenon is covered by the intrinsic electric and magnetic properties of the electrodes.

The preconditions for the derivation of the modified Maxwell's equations are: the sources and fields are assumed to be static or quasistatic; the volume conductor is finite and has inhomogeneous electrical conductivity $\sigma = \sigma(x,y,z)$ with the relative permittivity and permeability being assumed as those of free space i.e. $\varepsilon = \varepsilon_0$ and $\mu = \mu_0$.

Due to the static assumption, the arising electric field implies $\nabla \times \bar{E} = 0$. However, since water is a conducting medium, there exists an electromotive force (emf). Hence the Faraday's law equation becomes

$$\nabla \times \bar{E} = -j\omega\mu_0 \bar{H} + emf \tag{1}$$

where $\bar{E}$ is the electric field, $j$ is the imaginary unit, $\omega$ is the angular velocity, and $\bar{H}$ is the magnetic field intensity.

The Ampere's law equation accounts for current; however, in the case of the conducting media, the current is an impressed (applied) current designated by $\bar{J}^i$. Hence, the Ampere's law equation becomes

$$\nabla \times \bar{H} = j\omega\varepsilon_0 \bar{E} + \bar{J}^i \tag{2}$$

Due to the electrical conductivity of the water, the conduction current term $\sigma\bar{E}$ should be included on the right side of Equation 2 which becomes

$$\nabla \times \bar{H} = (\sigma + j\omega\varepsilon_0)\bar{E} + \bar{J}^i \tag{3}$$

By taking the divergence of Equation 3 on both sides, the equation becomes

$$\nabla \cdot \bar{E} = \frac{\nabla \cdot \bar{J}^i}{\sigma + j\omega\varepsilon_0} \tag{4}$$

The Gauss's law equation is inapplicable since conductors only have surface charge density.

Thus, Equation 4 represents the final modified Maxwell's equation applicable for scenarios where both relative permittivity and electrical conductivity need to be considered[11].

When employing a bare-electrode CCS over a specimen underwater, a two-port circuit is formed. The equivalent circuit model in Fig. 1 reveals $R_{eq}$ as the equivalent resistance. Its magnitude is influenced by the electrical conductivity of the water and the volume of water between the sensor and the specimen.

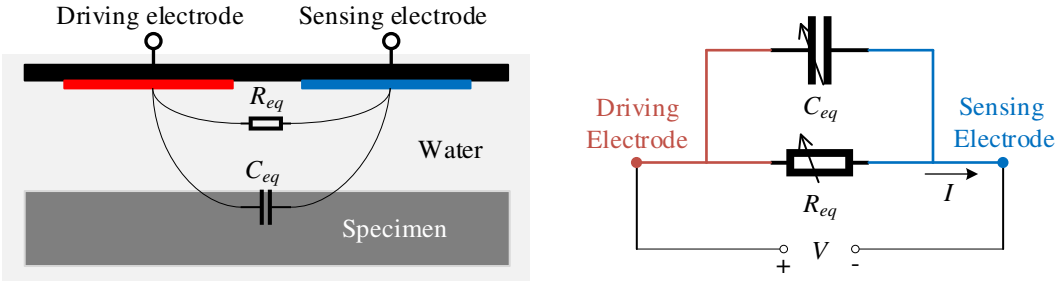


(a) (b)

**Fig. 1** Equivalent circuit model: (a) schematic of the CCS over specimen underwater; (b) schematic of the equivalent circuit model

Concurrently, $C_{eq}$ represents the equivalent capacitance which is dependent on the relative permittivity of the water and the specimen. The equivalent complex impedance between the two ports consists of two components; One is the impedance $\dot{Z}_R = R_{eq}$ generated by $R_{eq}$, and the other is the impedance $\dot{Z}_C = j\frac{1}{\omega C_{eq}}$ generated by $C_{eq}$. Thus, the final expression of $\dot{Z}_{eq}$ of the equivalent circuit is given by

$$\dot{Z}_{eq} = \frac{R_{eq}}{1+(\omega R_{eq} C_{eq})^2} + j\frac{\omega R_{eq}^2 C_{eq}}{1+(\omega R_{eq} C_{eq})^2} \tag{5}$$

Considering that $\dot{Z}_{eq}$ accounts for both electrical conductivity and relative permittivity as in Equation (5), the output current ($\dot{I}$) obtained from the sensing electrode emerges as the response to be monitored in the finite element simulations. $\dot{I}$ is expressed as

$$\dot{I} = \frac{\dot{V}}{\dot{Z}_{eq}} \tag{6}$$

where $\dot{V}$ is the sinusoidal voltage signal, which is the excitation.

## 3. Finite Element Simulations

The simulations were conducted using COMSOL Multiphysics® software (COMSOL). The Magnetic and Electric Fields (mef) module in COMSOL was employed because it offers the flexibility to account for both relative permittivity and electrical conductivity. The module also extends its capabilities to accommodate AC excitation.

### 3.1 Simulation Model Configuration

A water domain measuring 100 mm by 80 mm by 60 mm was modelled and assigned water properties. To enhance accuracy, an infinite domain was added. To simulate the non-conducting specimen, the relative permittivity of perspex, 3.4, was assigned to the specimen measuring 70 mm by 50 mm by 6 mm. The CCS substrate, measuring 25 mm by 15 mm by 1.5 mm, featured triangular electrodes with base and height dimensions of 8 mm, surrounded by a 1 mm width guard electrode as shown in Fig. 2. It was assigned FR4 (circuit board) material properties. A lift-off distance of 0.5 mm was left between the sensor and specimen.

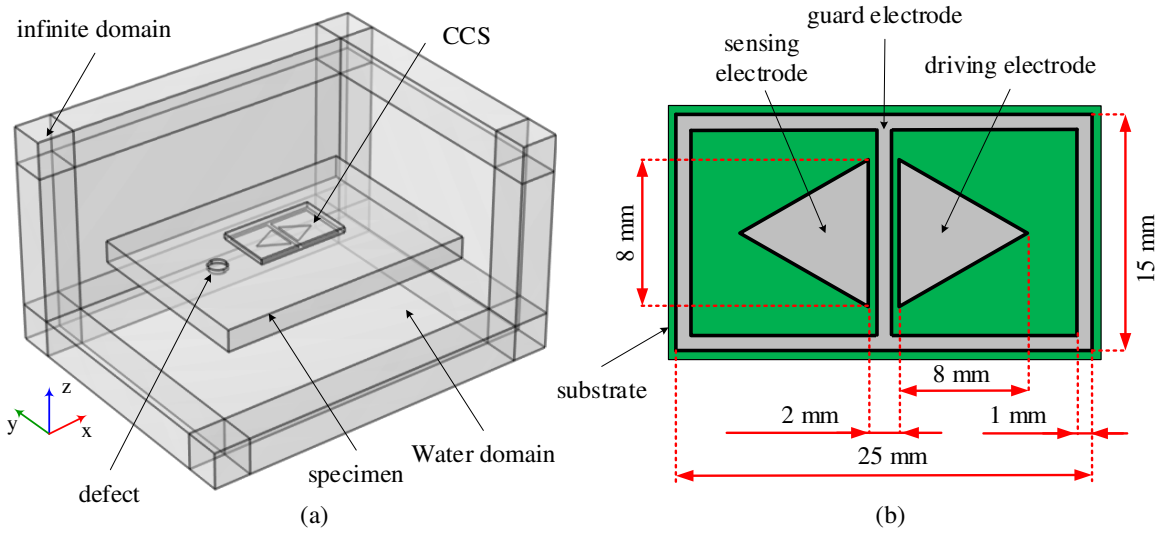


**Fig. 2** Simulation model: (a) water domain partially opened; (b) Schematic of CCS

For the insulated-electrode CCS, the insulation layer was modelled with a thickness of 0.1 mm and also assigned a relative permittivity of 3.4. The remaining parameters of the model of the insulated-electrode CCS remained the same as those of the bare-electrode CCS.

For the excitation, the driving and sensing electrodes were assigned voltages of 5 V and 0 V, respectively. A ground boundary condition was applied to the back of the CCS and the guard electrode. To achieve AC excitation, a frequency domain study was added, and a frequency of 100 kHz was assigned. The relative permittivity ($\varepsilon$), electrical conductivity ($\sigma$) and relative permeability ($\beta$) values of other model components used are summarized in Table 1[12–14].

**Table 1**. Parameters of the simulation model components

| Component | $\varepsilon$ | $\sigma$(S/m) | $\beta$ |
|---|---|---|---|
| FR4 circuit board | 4.5 | 0.004 | 1 |

| | | | |
|---|---|---|---|
| Non-conducting specimen | 3.4 | $1.0 \times 10^{-14}$ | 1 |
| Deionized water | 78.5 | $5.5 \times 10^{-8}$ | 0.999992 |
| Tap water | 79.25 | 0.0425 | 0.999992 |
| Sea water | 81 | 4 | 0.999992 |

## 3.2 Simulated Line Scans on Specimens in Deionized Water

Line scans were conducted for circular defects with a diameter of Ø5.0 mm. Defect depths varied from 1 mm to 5 mm in 1 mm intervals. In the model, the sensor was hovered over the specimen from left to right using a step-size of 1 mm. Once computation was complete, postprocessing was performed to obtain the sensor response, which is the terminal current.

From our previous study [15], the sensitivity distribution field (SDF) of the CCS in air was investigated in detail. The study revealed that the SDF comprises two sensitivity regions; the positive sensitivity value (PSV) region and the negative sensitivity value (NSV) region. The existence of the NSV region and its effects on sensor response was termed as the "Negative Sensitivity Phenomenon (NSP)". Placing an insulating specimen below the sensor was shown to perturb the SDF. What's more, the study showed that the presence of defects, and their size and location within the SDF have different extents of perturbation of the SDF, and this results in obtaining responses that have different patterns and characteristics. The study showed that responses can have a single trough, a single peak or a combination of both. For air as a medium, a response with a single trough signified that the PSV region was dominant around and within the defect. A single peak, on the other hand, showed that the NSV region was dominant. A response characterised by having both trough and peaks (peak-trough-peak effect) signified that both the PSV region and NSV region were present within and around the defect. The study showed that the magnitude and size of the peaks and troughs gave insight into which of the two regions had the greatest dominance. Furthermore, with the ideal boundary between the two regions termed as the critical point (primary critical point, $CP_P$), a second critical point (secondary critical point, $CP_S$) was discovered within the NSV region. In brief, the location of the defect in the different regions showed that obtaining a reverse trend in the variation of the response magnitude can be expected. As depth increases towards the $CP_P$, the sensor response decreases, tending towards zero. Beyond the $CP_P$, the response begins to increase until the depth reaches the $CP_S$. This is the first reverse trend. Increase in depth beyond the $CP_S$ results in a decrease in the sensor response. This is the second reverse trend. The findings of this previous study play a crucial role in understanding and explaining the findings of this current study as will be seen in the next section[15].

### 3.2.1 Non-conducting Specimen in Deionised Water

A comparison of the responses obtained from the two kinds of CCSs are shown in Fig. 3. The first observation is that the two sensors give responses that are characterized by single peaks. However, it should be noted that the curves exhibiting single peaks, unlike the troughs obtained in cases where air is the medium, is as a result of the higher relative permittivity of water (78.5 vs. 3.4 in the non-conducting medium). The relative permittivity of air, 1, is lower than that of the non-conducting medium. With this in mind, it is thus understood from the previous study[15], that the single peak characteristic here is because the positive sensitivity region dominates the SDF within and around the defects under water.

For the bare-electrode CCS, Fig. 3(a) reveals that the response increases with defect depth up to 3 mm, and the response remains consistent even at a depth of 4 mm. However, further increase in depth to 5 mm results in a lower response, indicating a reverse trend. In comparison, the responses from the insulated-electrode CCS in Fig. 3(b) follow the same trend; the responses increase with increase in depth and then the reverse trend begins, similarly at 3 mm. This reverse trend, as explained above, is an effect of the NSP.

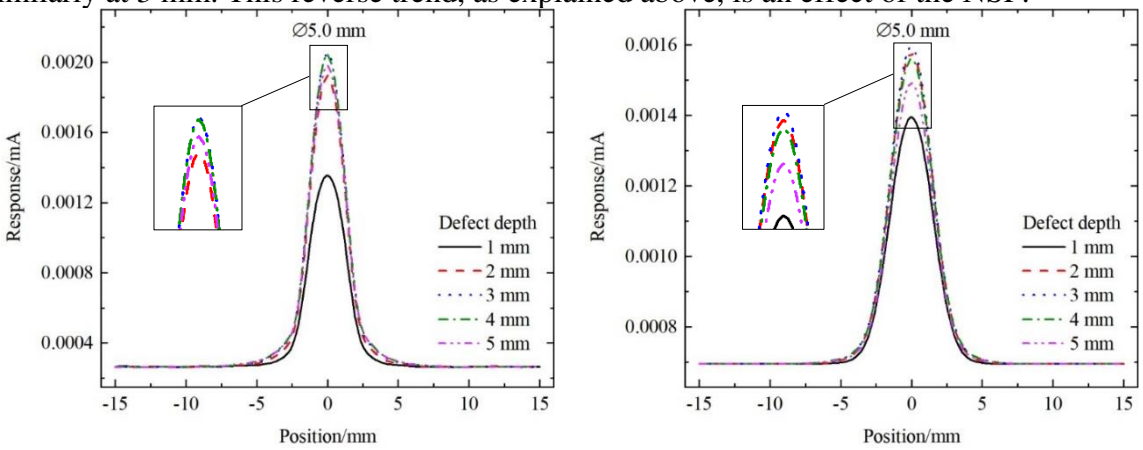


**Fig. 3** Responses for non-conducting specimen in deionized water: (a) Bare-electrode; (b) Insulated-electrode

### 3.2.2 Conducting Specimen in Deionised Water

Unlike non-conducting specimens, the electric field cannot penetrate conductors. From Fig. 4, it is seen that the responses are also characterized by single peaks. Whereas the shape of the responses in Fig. 3 is an overall effect of both the PSV and NSV regions, the shape in Fig. 4 is entirely determined by the NSV region. This is because electric field forms an equipotential surface which concentrates the NSV region at the bottom of the SDF.

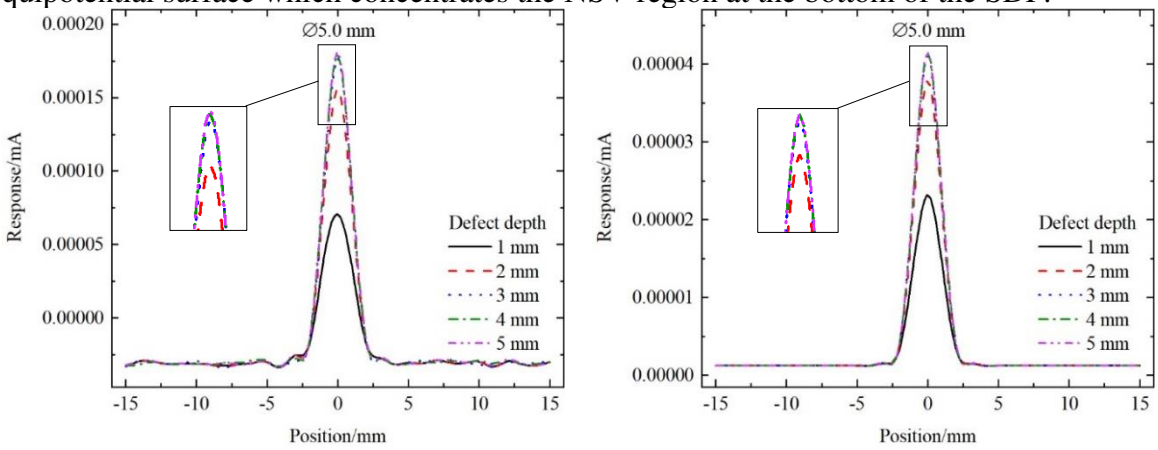


**Fig. 4** Responses for conducting specimen in deionized water: (a) Bare-electrode; (b) Insulated-electrode

In contrast to Fig. 3, the responses in Fig. 4(a) and Fig. 4(b) only increase with increase in depth. Also, the responses for the 3 mm, 4 mm, and 5 mm defects in **Error! Reference source not found.** seem to coincide for both CCSs, showing that these CCSs are not able to detect changes in depth greater than 3 mm for the conducting specimen.

## 3.3 Simulated Line Scans on Specimens in Tap Water

### 3.3.1 Non-conducting Specimen in Tap Water

Comparing results in Fig. 3 to those in Fig. 5, similar conclusions can be drawn for the case of the bare-electrode CCS.

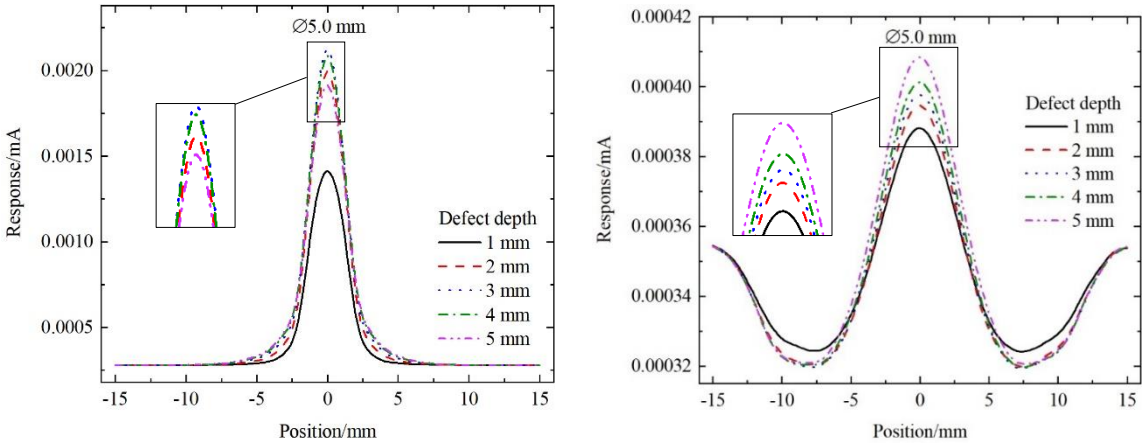


**Fig. 5** Responses for non-conducting specimen in tap water: (a) Bare-electrode; (b) Insulated-electrode

However, the responses from the insulated-electrode CCS show a significant difference. The responses in Fig. 5(b) show a unique shape resembling the peak-trough-peak effect—starting with a trough followed by a peak. This pattern is evidently a result of the NSP[15]. The coexistence of both troughs and peaks in Fig. 5(b) suggests tendency towards an overlap in the dominance of the two sensitivity value regions. The vast difference in the characteristics of the responses of the two CCSs shows that the effect of the NSP becomes much more pronounced when the insulation layer is present.

Notably, for the variation in response in Fig. 5(b), unlike previous cases with a reverse trend, it follows a uniform upward trajectory, increasing with defect depth. This signifies that defect is located between the $CP_P$ and the $CP_S$ where the NSV region is dominant over the PSV region. These differences in observations are attributed to both the presence of the insulation layer and the change in the electrical conductivity of the water.

### 3.3.2 Conducting Specimen Tap water

In Fig. 6, a consistent trend in response, akin to deionized water, is observed from the results of the bare-electrode sensor. The response values in Fig. 6 also seem consistent with those in deionized water, as seen in Fig. 4. However, unlike in deionized water, the results show that the bare-electrode CCS can detect a depth change of up to 5 mm.

For the case of the insulated-electrode CCS, the defect was not detectable. At this stage, the inability of the sensor to detect the defect can be attributed to be an effect of the higher electrical conductivity of the tap water, presence of the insulation layer, and/or the nature of the specimen. Further explanations are made based on subsequent findings.

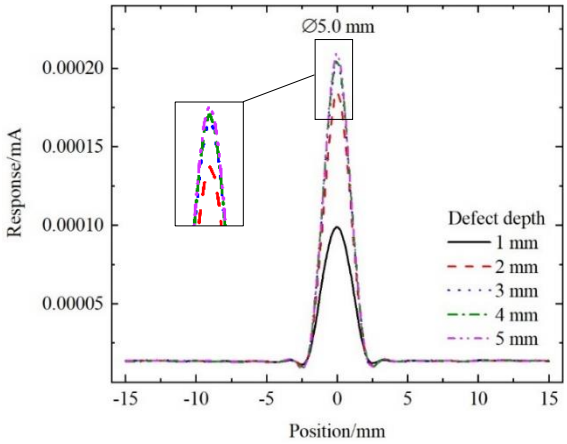


**Fig. 6** Responses conducting specimen in tap water using the bare-electrode CCS

## 3.4 Simulated Line Scans on Specimens in Sea Water

### 3.4.1 Non-conducting Specimen in Sea Water

For the bare-electrode CCS, the results in Fig. 7(a) are in line with findings of non-conducting specimens in previous sections. The reverse trend however begins at the 5 mm defect depth as represented by the consistent response values with the 4 mm defect depth. This difference shows that in different kinds of water, the SDF is perturbed differently.

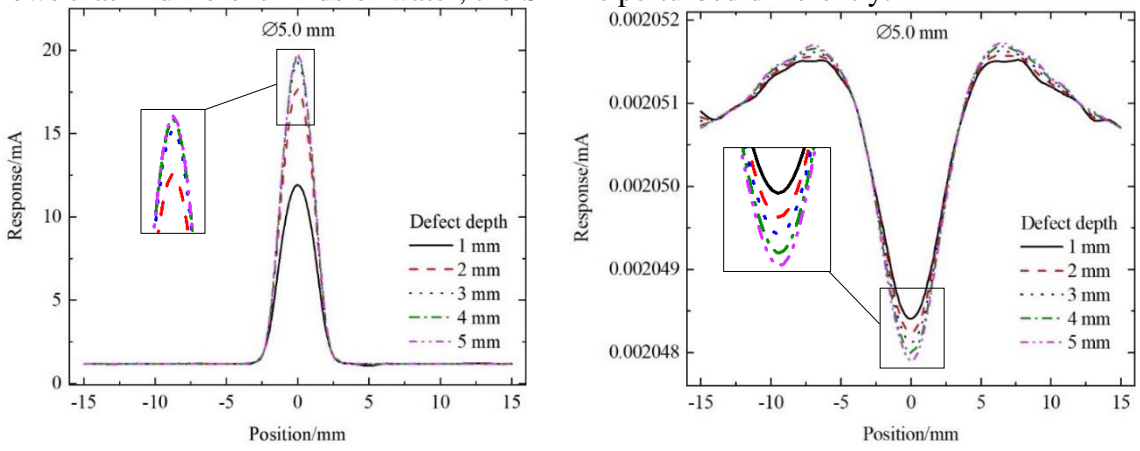


**Fig. 7** Responses for non-conducting specimen in sea water: (a) Bare-electrode; (b) Insulated-electrode

For the insulated-electrode CCS, the results in Fig. 7(b), also diverge from the trends observed in previous simulations. Specifically, the responses obtained are characterized by a major trough bordered by peaks on either side. This is also indicative of the peak-trough-peak effect that arises as a result of tendency towards a shift in dominance between the two sensitivity value regions. This difference in the shape of the responses is similarly attributed to both the presence of the insulation layer and the high electrical conductivity of the sea water. Also, for the variation in responses, it is observed that the change in response of the insulated-electrode CCS increases with increase in defect depth.

### 3.4.2 Conducting Specimen in Sea Water

Unlike in deionized water, the defect was not detectable by both kinds of CCSs in sea water. At this stage, this is attributed to the high conductivity of sea water and/or the nature of the

specimen.

In this feasibility study, it is hypothesized that the nature of the water is mainly responsible for this observation. Sea water, with its very high conductivity, behaves like a conductor itself, preventing electric field penetration. However, given the preliminary nature of these studies, it can be stated that further investigation, particularly in simulating conducting specimens in sea water, is necessary.

Conversely, all other simulation results of the specimen cases, aside from some cases of the conducting specimen in tap and sea water, demonstrate that both kinds of CCSs are able to detect and characterize defects by size. This indicates the feasibility of performing underwater NDE using the coplanar capacitive sensing technique.

Having established the feasibility of underwater inspection through simulation modeling, the next crucial step involves conducting proof-of-concept experiments.

## 4. Experiments

For the experiments, both a non-conducting (perspex) and conducting specimen (aluminum alloy 7075) featured machined defects with matching size and orientation. Unlike simulations, our experiments focused on depths from 1 mm to 3 mm, a deliberate choice considering uncertainties like unforeseen human and environmental factors and electrical equipment stability fluctuations. This limitation was made to mitigate potential variations. Fig. 8 illustrates the orientation of the defects and their dimensions.

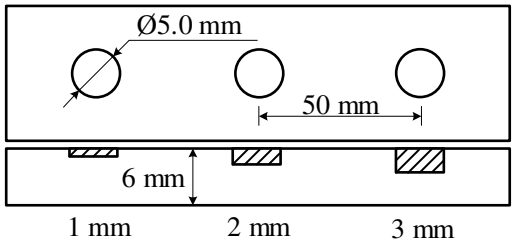


**Fig. 8** Schematic showing dimensions of the specimens used for the experiments

The fabricated CCS electrodes precisely mirrored the dimensions and orientation of those in the simulations. The two variants of the CCS are shown in Fig. 9.

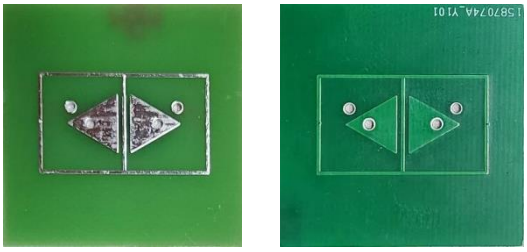

(a) (b)

**Fig. 9** Fabricated sensor substrates: (a) Bare-electrode CCS; (b) Insulated-electrode CCS

Non-conductive shells were made for the sensor substrates. A lab-prepared waterproof sealant was poured around the slots, leaving electrodes uncovered. After a two-day conditioning period, the sensors were ready for the experiments.

### 4.1 Experimental Setup

Fig. 10 illustrates the experimental setup. A Tektronix function generator (model AFG1022)

was employed to produce a 5 V excitation at a frequency of 100 kHz for the driving electrode. The sensing electrode was linked to a custom transimpedance amplifier. The amplifier output was connected to a DSP lock-in amplifier (model OE2042) synchronized with a 5 V-100 kHz reference signal. This lock-in amplifier was interfaced with a computer used for controlling probe movement and data collection.

To minimize stray capacitances, a grounded unflawed conducting plate was placed on the base of the scanning stage beneath the water trough. The specimen was placed inside the water trough measuring 350 mm by 260 mm by 155 mm, with walls of equal thickness measuring 3 mm. After ensuring that a lift-off of approximately 0.5 mm was left, water was added to the water trough. For safety considerations, water was maintained at a height of 35 mm for all the subsequent experiments. After ensuring that the specimen was well-adhered to the bottom surface of the water trough, the experiments were then conducted.

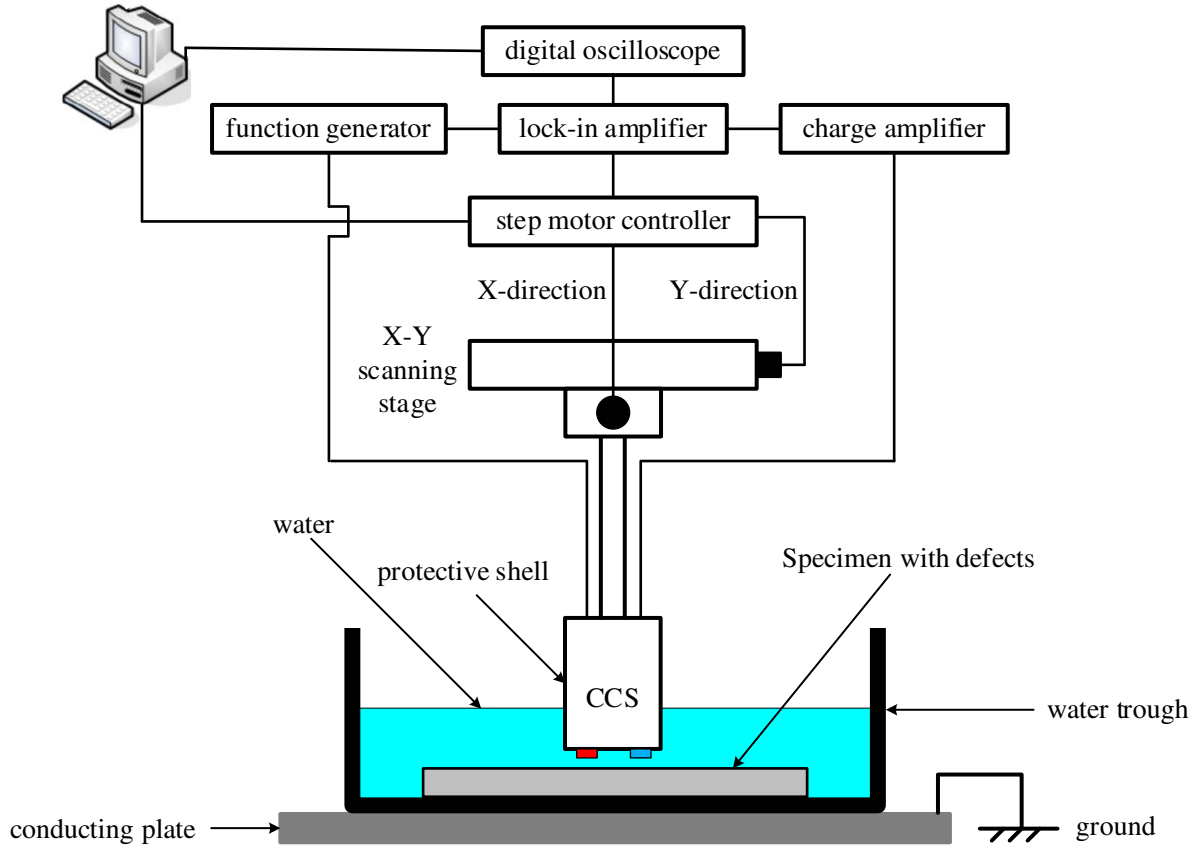


**Fig. 10** Schematic of the experimental setup

## 4.2 Experiments on Specimens in Deionized Water

Commercially available deionized water was acquired. The deionized water adhered to grade 1 standards, with an electrical conductivity of less than 5.5 x $10^{-8}$ S/m.

### 4.2.1 Non-conducting Specimen in Deionized Water

In the experiments, the response obtained from the CCS was a voltage response. Although the raw data from the line scans showed that defects were detectable, the variation trend was unclear. Consequently, a data processing technique, outlined in [15], yielded the final processed data shown in Fig. 11.

For the bare-electrode CCS, it is seen from Fig.11(a) that the response increases with increase in defect depth until 2 mm. However, the response reduces when depth increases to 3 mm, exhibiting a reverse trend as in the simulations in Fig. 3(a). For the insulated-electrode CCS, Fig. 11(b) shows that the response increases with increase in depth. However, the maximum response magnitude of the 3 mm defect is much closer to that of the 2 mm defect. This signifies tendency towards the reverse trend. Fig. 11(b) also reveals that the peak-trough-peak effect is present.

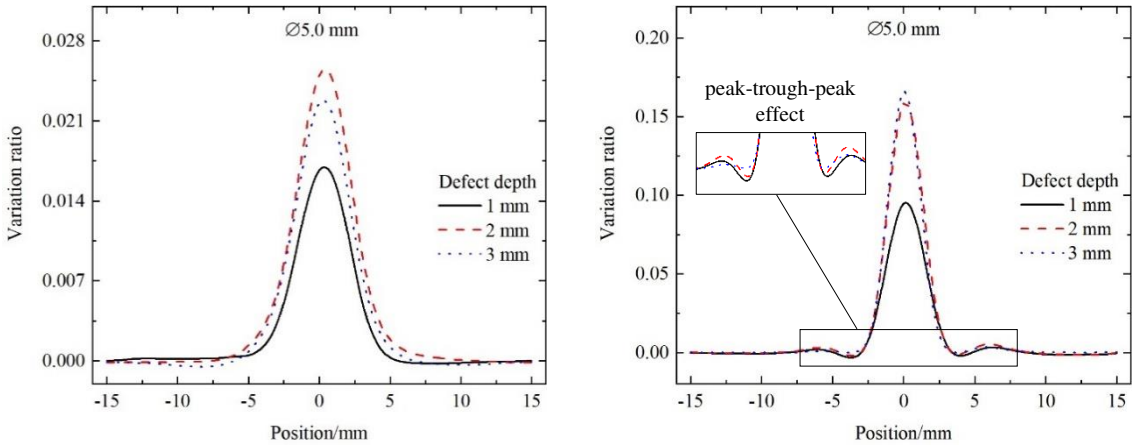


**Fig. 11** Processed data for non-conducting specimen in deionized water: (a) Bare-electrode; (b) Insulated-electrode

To further assess the feasibility with regard to imaging, surface scans were performed as shown in Fig. 12 and Fig. 13.

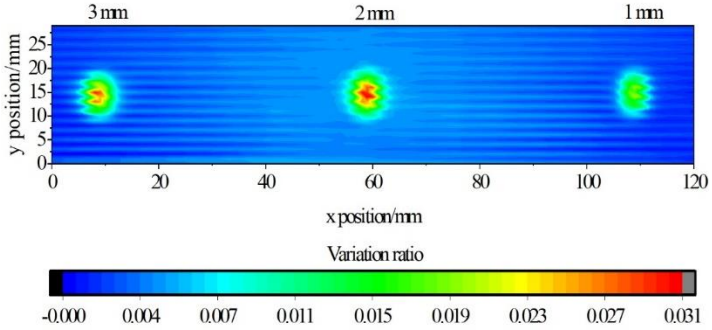


**Fig. 12** Surface scan obtained using bare-electrode CCS for non-conducting specimen in deionized water

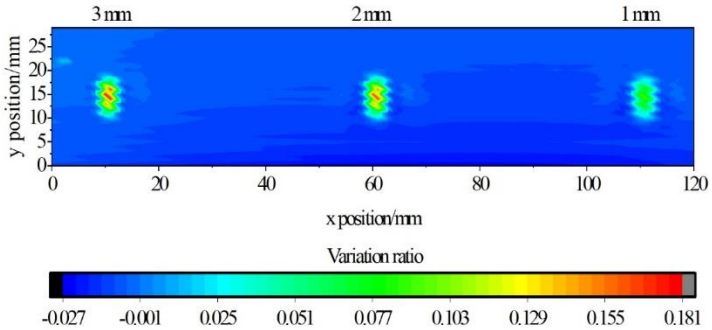

**Fig. 13** Surface scan obtained using insulated-electrode CCS for non-conducting specimen in deionized water

The defect images seem to display a circular nature. For the bare-electrode CCS, a comparison of the intensities in Fig. 12 shows that the reverse trend similarly occurs at a depth greater than 2 mm. For the insulated-electrode CCS, Fig. 13 shows that the response increases with increase in defect depth. This difference, as mentioned earlier, is attributed to the presence of the insulation layer.

### 4.2.2 Conducting Specimen in Deionized Water

The results in Fig. 14 show that response increases with increase in defect depth as similarly observed from Fig. 4. The responses in Fig. 14 show troughs on either side of the peaks. This phenomenon, although not as pronounced, also appears to be present in the simulation results in Fig. 4 and Fig. 6.

From the surface scans in Fig. 15 and Fig.16, it is also evident that the two kinds of CCSs are capable of defect detection and capacitive imaging in deionized water.

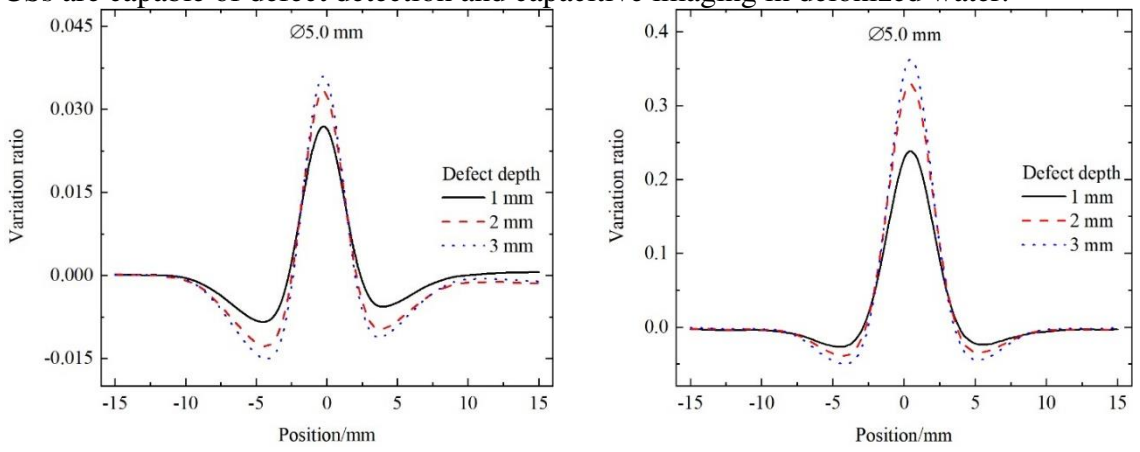


**Fig. 14** Processed data for conducting specimen in deionized water: (a) Bare-electrode; (b) Insulated-electrode

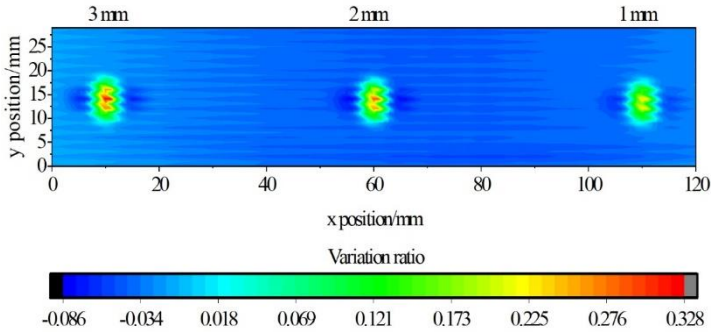


**Fig. 15** Surface scan obtained using bare-electrode CCS for conducting specimen in deionized water

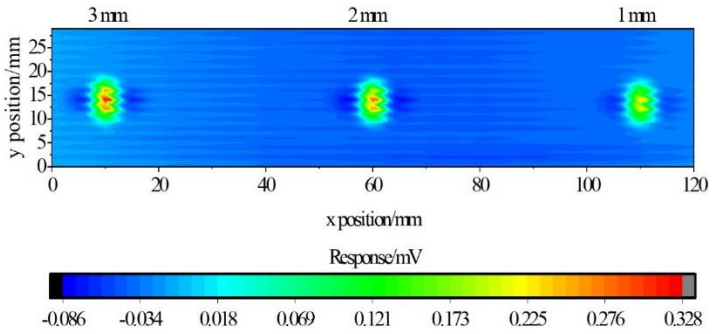


**Fig. 16** Surface scan obtained using insulated-electrode CCS for conducting specimen in deionized water

The blue shades on the sides of the defects are synonymous to the troughs observed in the line scans in Fig. 14.This phenomenon was observed in earlier research[16]. The pattern from the image was named as the "butterfly pattern" and the results of that study showed that this phenomenon arises because the conducting specimen is a floating conductor. In this feasibility study, grounding of the immersed conducting specimen itself was not done as preliminary experiments showed that it made defect detection rather challenging.

Generally, the experimental results provide validation that both kinds of CCSs can feasibly perform NDE of materials in deionized water.

## 4.3 Experiments on Specimens in Tap water

All other parameters were kept the same as in the case of deionized water.

### 4.3.1 Non-conducting Specimen in Tap water

Fig. 17 reveals a notable pattern distinct from that obtained in the simulation results in Fig. 5—the pronounced peak-trough-peak pattern.

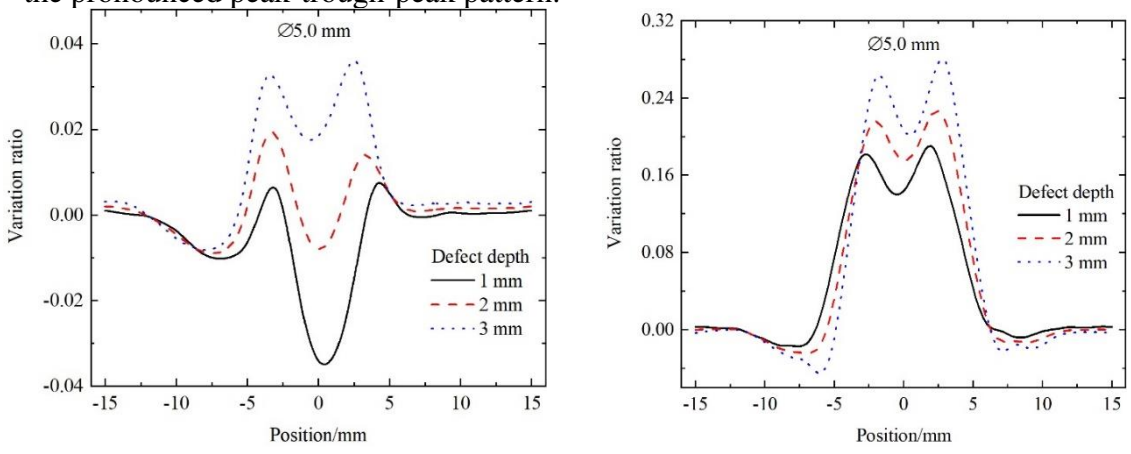


**Fig. 17** Processed data for non-conducting specimen in tap water: (a) Bare-electrode; (b) Insulated-electrode

This discrepancy is attributed to the difference in conditions between simulations and experiments. The peak-trough-peak pattern in Fig. 17 are simply indicative of the tendency towards a shift in dominance between the two sensitivity value regions as in the case of Fig. 5(b) and Fig. 7(b).

For the bare-electrode sensor, referencing the center as a focal point, the response magnitude in Fig. 17(a) exhibits a decrement from 1 mm to 2 mm depth, followed by an increment at 3 mm depth. This reverse trend is similarly attributed similarly to the NSP. In the ideal scenario where the $CP_P$ is situated at a zero-variation ratio, the 1 mm defect is predominantly situated within the PSV region. Contrastingly, the 2 mm depth defect experiences a relatively equitable distribution between PSV and NSV regions. The 3 mm depth defect is predominantly immersed in the NSV region. However, for the insulated-electrode CCS, the response magnitudes in Fig. 17(b) increase with increase in defect depth and this difference is attributed to the presence of the insulation layer. The responses also exhibit the peak-trough-peak effect.

From the surface scans in Fig. 18 and Fig. 19, it is seen that the images of the defects obtained using the bare-electrode CCS possess a more circular nature. The defect images in Fig. 19 are horizontally dispersed. This dispersion can be attributed to the presence of the thin insulation layer and also the high electrical conductivity of the water which significantly affect the sensitivity distribution within the SDF. Nevertheless, the varying intensities of shades at the defect centers indicate differences in depth.

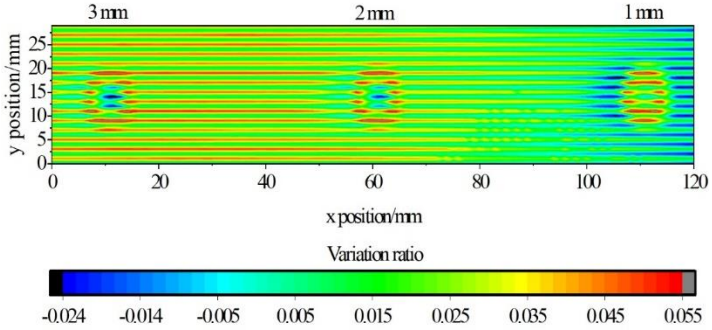


**Fig. 18** Surface scan obtained using bare-electrode CCS for non-conducting specimen in tap water

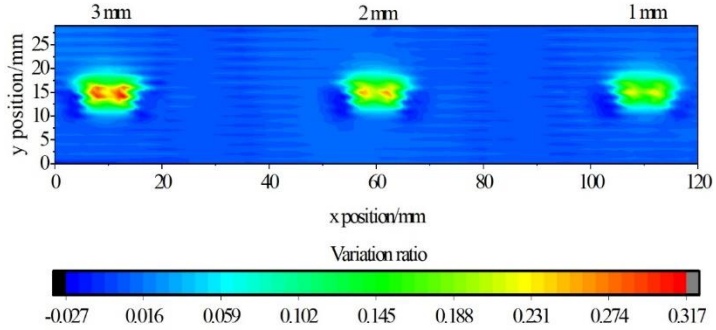


**Fig. 19** Surface scan obtained using insulated-electrode CCS for non-conducting specimen in tap water

### 4.3.2 Conducting Specimen in Tap water

Unlike in simulations, experiments show that both CCSs can detect the defects. Fig. 20 shows that the response increases with increase in defect depth as observed in the simulations.

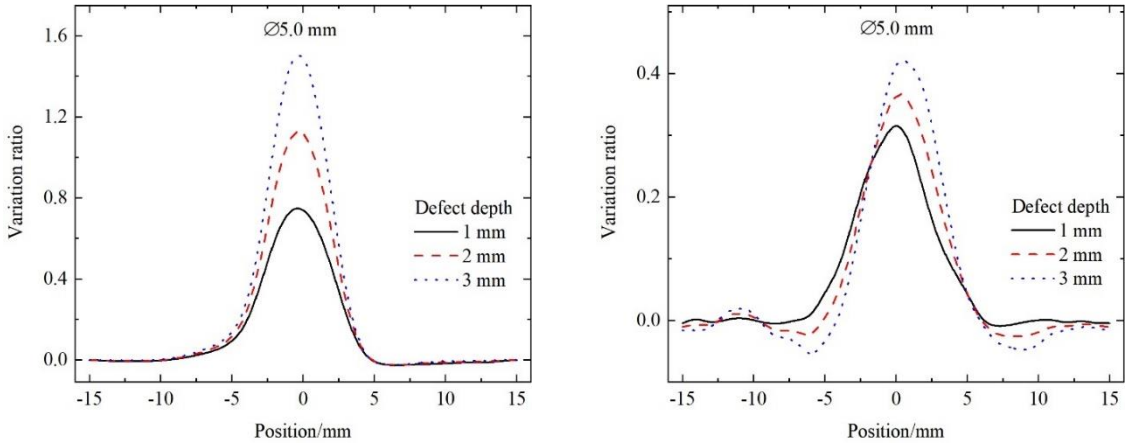


(a) (b)

**Fig. 20** Processed data for conducting specimen in tap water: (a) Bare-electrode; (b) Insulated-electrode

The surface scans in Fig. 21 and 22 similarly exhibit a circular nature, and the varied intensities of shades at the defect centers indicate depth variations. This experimental evidence substantiates the feasibility of detecting, characterizing and imaging surface defects immersed under tap water using CCSs.

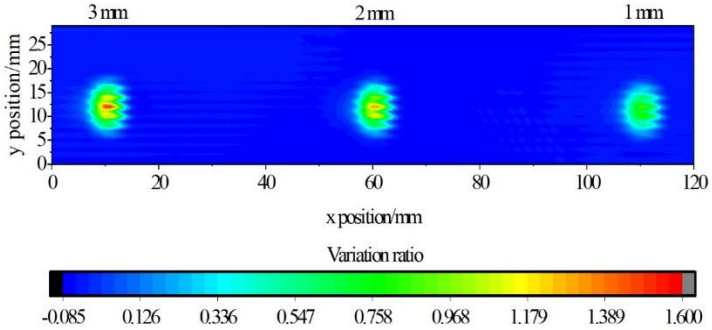


**Fig. 21** Surface scan obtained using bare-electrode CCS for conducting specimen in tap water

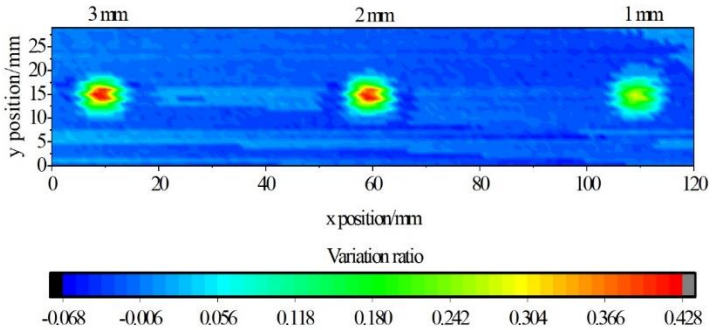


**Fig. 22** Surface scan obtained using insulated-electrode CCS in tap water

## 4.4 Experiments on Specimens in Sea water

Sea water was obtained from the Yellow sea around the coastal area of Qingdao city in Shandong province, China. All other parameters were kept the same as in the case of deionized water.

### 4.4.1 Non-conducting Specimen in Sea Water

Fig. 23(a) and 23(b) show that the response obtained in sea water increases with increase in

defect depth.

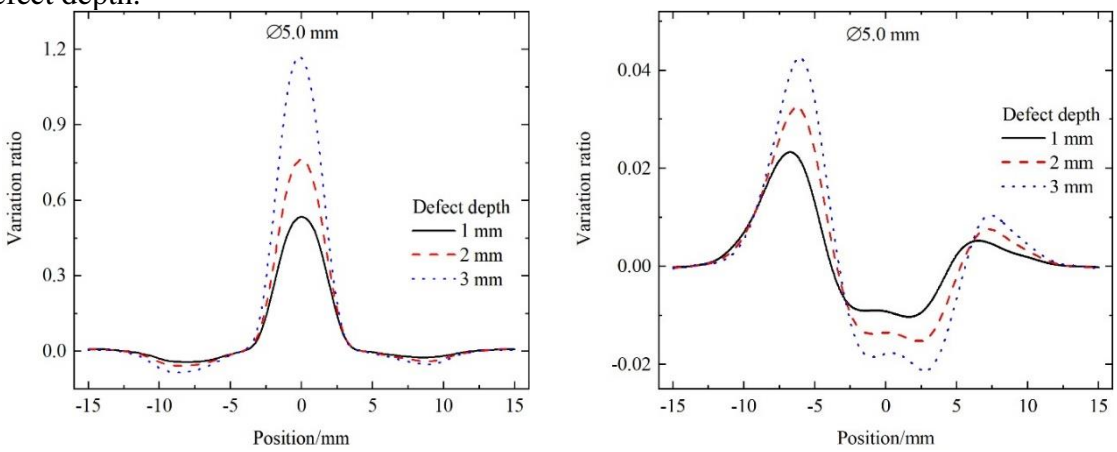


**Fig. 23** Processed data for non-conducting specimen in sea water: (a) Bare-electrode; (b) Insulated-electrode

For the bare-electrode, unlike the responses in Fig. 17(a), Fig. 23(a) demonstrates that the effect of the NSP is not as prominent signifying that the SDF is majorly dominated by the PSV region resulting in single peaks.

For the insulated-electrode CCS, the curves in Fig. 23(b) are characterized by the peak-trough-peak effect showing that the NSV region is dominant as in the simulation results in Fig. 7(b). This shows that presence of the insulation layer significantly affects the response.

The surface scan results in Fig. 24 and Fig. 25 similarly demonstrate that the two CCSs are capable of defect detection, characterisation and imaging of non-conducting specimens immersed in sea water.

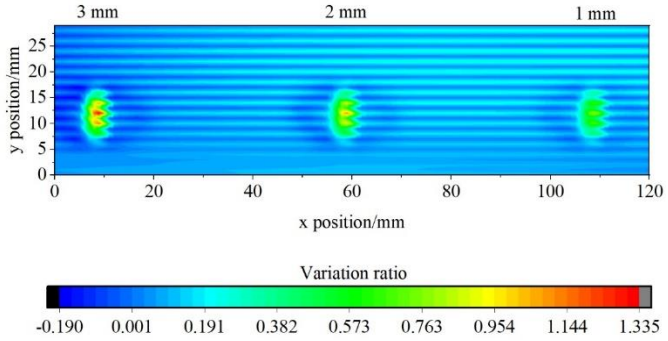


**Fig. 24** Surface scan obtained using bare-electrode CCS for non-conducting specimen in sea water

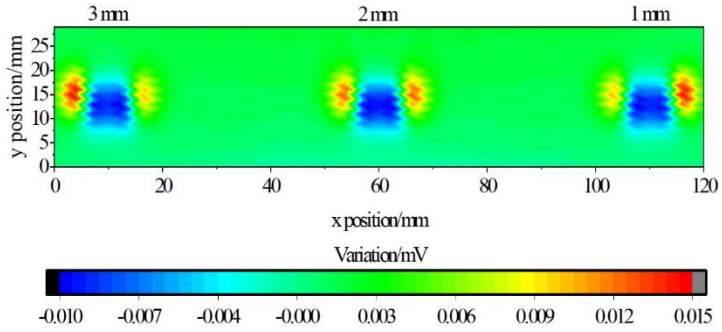


**Fig. 25** Surface scan obtained using insulated-electrode CCS for non-conducting specimen in sea water

### 4.4.2 Conducting Specimen in Sea Water

As in the simulations, the defects were undetectable by the bare-electrode sensor in experiments, even when using different frequencies.

Similarly, defects were undetectable in initial experiments carried out using the insulated-electrode CCS at 100 kHz. However, by sweeping through a number of frequencies, it was found that defects were detectable at 60 MHz as seen from Fig. 26. What's more, they can be characterized by depth. This is unlike in simulations where despite varying the excitation frequency, detection of defects seemed impossible for the conducting specimen. This discrepancy between simulations and experiments is attributed to differences in conditions, ideal versus real.

Remarkably, the pattern of the responses in Fig. 26 is much different from the responses obtained for other conducting specimens in this study. This pattern at the moment, is attributed to being a result of the conducting nature of the specimen, the high conductivity of the sea water and/or the presence of the insulation layer.

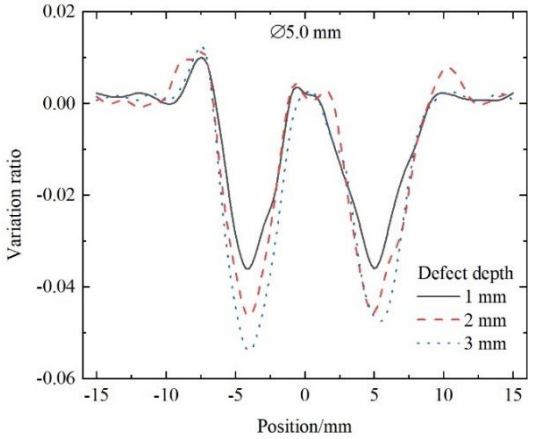


**Fig. 26** Processed data for conducting specimen obtained using the insulated-electrode CCS in sea water

The surface scan in Fig. 27 validates the feasibility of using insulated-electrode CCS for underwater NDE in sea water given the varying intensities of the regions representing the defects.

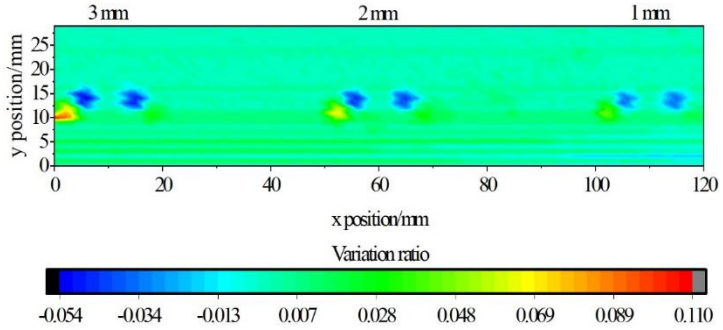


**Fig. 27** Surface scan obtained using insulated-electrode CCS for conducting specimen in sea water

Overall, the experimental results obtained in this study validate the assertion made by pioneer scholars that the coplanar capacitive technique is capable of underwater inspection. The technique demonstrates the capability of obtaining proficiency in defect detection, characterisation and capacitive imaging in underwater environments. Further discussions on the simulation and experimental results are presented in the next section.

## 5. Discussions

Generally, the simulations and experiments demonstrate that CCSs are capable of gauging structural integrity in underwater environments. The results collectively emphasize that despite variations in sensor response magnitude, primarily attributable to differences in medium properties, the presence of an insulation layer significantly influences the response in cases where the electrical conductivity is high, especially for non-conducting materials.

The results also show that despite the physical implication of the bare-electrodes, the general physical properties and characteristics of the electric field in water remain consistent. SDFs of both CCSs exhibit PSV and NSV regions, with dominance determined by the material under test, as well as the location, size, and shape of defects.

A more intricate challenge arose when dealing with conducting specimens. Defects could not be detected in some instances. However, with meticulous adjustments to excitation parameters, advanced equipment, and enhanced signal processing techniques, it is anticipated that the defects can be detected. This optimism underscores the need for further studies.

From the surface scan images, characterizing defects, especially by shape, proves challenging especially for the insulated-electrode CCS. These differences in image quality may otherwise arise from factors like high lift-off, interference, as well as fluctuations in equipment stability. While image processing techniques can enhance image quality and detail, meticulous measures to minimize these uncertainties are crucial.

Further studies are necessary to comprehensively assess the advantages and disadvantages of each type of CCS in underwater NDE. Currently, a notable advantage of the insulated-electrode CCS is its ability to protect electrodes. This proves particularly valuable in preventing corrosion of the electrodes. Nevertheless, the capability for underwater inspection not only opens avenues for custom underwater CCS design but also encourages research on enhancing CCS performance or other capacitive sensors specifically designed for underwater environments.

Generally, this study suggests the technique's applicability to a wide range of materials used in aquatic environments. The study also paves the way for numerous research opportunities in various research fields related to underwater NDE using capacitive technology, such as examining corrosion under insulation, detecting water intrusion, structural health monitoring in underwater environments and more.

## Conclusions

In this study, the feasibility of employing CCSs for underwater NDE was explored. Examining the fundamental theory and principles of underwater inspection showed that electrical conductivity has a significant influence. Investigations were conducted on two types of CCSs to assess their performance in detecting defects in both conducting and non-conducting specimens. In general, experimental validation of the simulation results demonstrated the feasibility of underwater NDE using both types of CCSs, affirming assertions made by pioneer scholars. This study contributes to expanding the knowledge base of underwater NDE techniques by presenting CCSs as a viable alternative. Future research endeavors in this domain will encompass the underwater inspection of various kinds of composite materials, corrosion detection under insulation, the design and enhancement of custom CCSs for underwater applications, and development and optimization of CCS-support systems for underwater use, among other areas.

## Acknowledgements

Not applicable.

## Availability of Data and Materials

The datasets used or analysed during the current study are available from the corresponding author on reasonable request.

## Competing Interests

The authors declare that they have no known competing financial interests or personal relationships that could have appeared to influence the work reported in this paper.

## Funding

This work was supported in part by the National Natural Science Foundation of China under Grant 52075549 and in part by Grant 52005512; and in part by the Fundamental Research Funds for the Central Universities under Grant 22CX01003A-6.

## Authors' Contributions

Martin Mwelango: Conceptualization, methodology, sourcing and formal analysis of relevant references, Finite Element simulations, experiment design and setup, experiments, writing – original draft; Mingrui Zhao and Ruixiang Fan: Methodology, finite element simulations, experiment design and setup; Zhaorui Zhang: experiment design and setup, sensor fabrication, and design of custom transimpedance amplifier; Zong Kai and Pengcheng Ma: Finite element simulations; Xiaokang Yin, Xin'an and Wei Li: Conceptualization, Methodology, Writing – editing, supervision of the whole process. All authors read and approved the final manuscript.

## References

[1] Diamond GG, Hutchins DA. A new capacitive imaging technique for NDT. In Proceedings of the European Conference on NDT 2006;25-29.

[2] Diamond GG, Hutchins DA, Gan TH, Purnell P, Leong KK. Single-sided capacitive imaging for NDT. Insight 2006;48(12):724-30. https://doi.org/10.1784/insi.2006.48.12.724

[3] Dutta A, Bera SK, Saha S, Mandal H, Dey C, Bera SC. Study of a noncontact flow transducer using semicylindrical capacitive sensor. IEEE Trans Instrum Meas. 2020 Sep https://doi.org/16;70:1-0. 10.1109/TIM.2020.3024027

[4] Cui Z, Wang H, Chen Z, Yang W. Image reconstruction for field-focusing capacitance imaging. Meas Sci Technol. 2011 Feb 15;22(3):035501. https://doi.org/10.1088/0957-0233/22/3/035501

[5] Xie CG, Stott AL, Plaskowski A, Beck MS. Design of capacitance electrodes for concentration measurement of two-phase flow. Meas Sci Technol. 1990;1(1):65. https://doi.org/10.1088/0957-0233/1/1/012

[6] Iliyasu AM, Shahsavari MH, Benselama AS, Nazemi E, Salama AS. An optimised and novel capacitance-based sensor design for measuring void fraction in gas–oil two-phase flow systems. Nondestruct Test Eval. 2024 Jan 10:1-7. https://doi.org/10.1080/10589759.2023.2301492
[7] Li N, Liu K, Yang X, Cao M. Research on application of wax deposition detection in the nonmetallic pipeline based on electrical capacitance tomography. J Sens. 2016 Jul;2016. https://doi.org/10.1155/2016/7390470
[8] Wrasse AD, Bertoldi D, Morales RE, da Silva MJ. Two-phase flow rate measurement using a capacitive sensor and a Venturi meter. In 2017 IEEE Sensors 2017; 1-3. https://doi.org/10.1109/ICSENS.2017.8234150
[9] Hu X, Yang W. Planar capacitive sensors–designs and applications. Sens Rev 2010; 26;30(1):24-39. https://doi.org/10.1108/02602281011010772
[10] Fleisch D (2008) A student's guide to Maxwell's equations. England.
[11] Malmivuo J, Plonsey R (1995) Bioelectromagnetism: principles and applications of bioelectric and biomagnetic fields. USA.
[12] Wang Q, Cha CS, Lu J, Zhuang L. Ionic conductivity of deionized water in charged porous matrix. ChemPhysChem 2012;13(2):514-9. https://doi.org/10.1002/cphc.201100784
[13] Emerson Process Management. Application data theory application of conductivity. https://www.emerson.com/documents/automation/application-data-sheet-theory-application-of-conductivity-rosemount-en-68442.pdf; 2010 [accessed 20 July 2023].
[14] The Engineering ToolBox. Electrical Conductivity - Elements and other Materials. https://www.engineeringtoolbox.com/conductors-d_1381.html; 2008 [accessed 20 July 2023].
[15] Mwelango M, Yin X, Zhao M, Zhang Z, Han Z, Fan R, Yuan X, Li W. Investigations into the negative sensitivity phenomenon in the detection of hidden defects using coplanar capacitive sensors. NDT E Int. 2023;102962. https://doi.org/10.1016/j.ndteint.2023.102962
[16] Yin X, Hutchins DA, Chen G, Li W. Detecting surface features on conducting specimens through an insulation layer using a capacitive imaging technique. NDT E Int 2012;52:157-66. https://doi.org/10.1016/j.ndteint.2012.08.004

## Author Biographies

Martin Mwelango received his B.Eng. degree in 2016 and M.Sc. degree in 2021 from China University of Petroleum (East China), Qingdao, China where he is currently pursuing a Ph.D. degree in Safety Science and Engineering. His research interests include Design and novel applications of coplanar capacitive sensors in non-destructive testing, novel non-destructive evaluation and SHM techniques.

Xiaokang Yin received his B.Eng. degree from East China University of Science and Technology (ECUST), Shanghai, China, in 2005. He continued his postgraduate studies at the University of Warwick, Coventry, UK, where he obtained his M.Sc. degree in 2007 and Ph.D. degree in 2011. He then joined China University of Petroleum (East China), where he is currently a Professor in the School of Mechanical and Electronic Engineering. His research interests include novel non-destructive evaluation and SHM techniques.

Mingrui Zhao received his B.Eng. degree from China University of Petroleum (East China), Qingdao, China, in 2022. He is currently working toward the Ph.D. degree in Safety Science and Engineering in China University of Petroleum (East China), Qingdao, China. His research interests include sensor design, signal processing and novel electro-magnetic non-destructive evaluation techniques.

Zhaorui Zhang received the B.Eng. degree from China University of Petroleum (East China), Qingdao, China, in 2021. He is currently working toward the M.E. degree in mechanical engineering in China University of Petroleum (East China), Qingdao, China. His research interests include sensor design and test system design for novel electro-magnetic non-destructive testing.

Zongkai Han received his B.Eng. degree from China University of Petroleum (East China), Qingdao, China, in 2022. He is currently working toward the M.E. degree in mechanical engineering in China University of Petroleum (East China), Qingdao, China. His research interests include research and design of aging evaluation systems for non-metallic materials

Ruixiang Fan received his B.Eng. degree from China University of Petroleum (East China), Qingdao, China, in 2022. He is currently working toward the M.E. degree in mechanical engineering in China University of Petroleum, Qingdao, China. His research interests include multi-electrode capacitive sensor design and test system design for novel electro- magnetic non-destructive testing.

Pengcheng Ma received the B.Eng degree from Yantai University,Yantai,China,in2023. He is currently working toward the M.E. degree in mechanical engineering in China University of Petroleum (East China), Qingdao, China. His recearch interests include Design of capacitive and novel electro- magnetic non-destructive testing techniques.

Xin'an Yuan received his B.Eng., M.E. and Ph.D. degrees in Mechanical Design Manufacture and Automation from China University of Petroleum (East China), Qingdao, China, in 2013, 2016 and 2019 respectively. He then joined China University of Petroleum (East China). He is currently an Associate Professor in the research institute of School of Mechanical and Electronic Engineering. His research interests include non-destructive testing, signal processing and deep learning.

Wei Li received his Ph.D. degree in mechanical and electronics engineering from the China University of Petroleum (East China), Qingdao, China in 2007. Following graduation, he joined the China University of Petroleum, where he is currently a Professor in the School of Mechanical and Electronic Engineering. His current research interests include electro-magnetic non-destructive evaluation and signal processing, offshore engineering structure design and FEM analysis, and pipeline safety and re